Dendrochronologia 94 (2025) 126399

Contents lists available at ScienceDirect

Dendrochronologia

journal homepage: www.elsevier.com/locate/dendro

Exploring potential drivers of divergence in tree-ring based temperature reconstructions of NW North America

Marcel Kunz [a,*], Rob Wilson [b], Emily Reid [b], Eileen Kuhl [c], Jan Esper [a,d]

[a] Department of Geography, Johannes Gutenberg University, Mainz 55128, Germany
[b] School of Earth and Environmental Sciences, University of St. Andrews, Scotland KY16 9AJ, UK
[c] Deutscher Wetterdienst (German Meteorological Service), Offenbach 63067, Germany
[d] Global Change Research Institute of the Czech Academy of Sciences (CzechGlobe), Brno 61300, Czech Republic

ARTICLE INFO

Keywords:
Dendroclimatology
Density
Blue intensity
Ring width
Climate change
Temperature
Gridded data
Detrending

ABSTRACT

Non-stationary growth responses have been identified in tree-ring width (TRW) and maximum latewood density (MXD) chronologies of north-west North America. Here, we present MXD and latewood blue intensity (LWBI) data from two areas of the Yukon Territory (YT) to explore divergent climate-growth relationships until 2021 CE and evaluate the underlying reasons considering different detrending methods and instrumental datasets. We examine divergent long-term trends and changing inter-annual signals using well-replicated chronologies integrating a mixture of young and mature trees. Both tree-ring parameters correlate significantly ($p < 0.05$) with May–August temperatures, but the MXD results are stronger and show less divergence in trend. Variability among differently detrended MXD chronologies is smaller and a signal-free version of age-dependent spline detrending appears to be optimal for both YT sites. Comparison of instrumental data products reveals that the highest and most stable correlations are achieved using the Berkeley Earth dataset. Additionally, using different sub-diurnal temperatures affects both trend and correlation divergence with maximum temperature consistently showing the strongest and minimum temperature the weakest results. We conclude that regional divergence in the YT is characterized by trend rather than high-frequency issues and is larger in LWBI than MXD data. Altering detrending methods and diurnal temperatures is of greater importance than varying instrumental data products. Most stationary responses are recorded when applying signal-free age-dependent spline detrending to tree-ring data and targeting Berkeley Earth maximum temperatures. Disregarding these methodological choices may amplify divergence in YT MXD and LWBI calibration models.

1. Introduction

Uniformitarianism implies a temporally stable relationship between environmental factors and tree growth and has been an essential principle of dendroclimatological research for many decades (Fritts, 1976; Wilmking et al., 2017). However, weakening climate responses of previously temperature-limited sites in several regions of the Northern Hemisphere in recent decades (often referred to as the "divergence problem" (DP)) have challenged this assumption and questioned the value of tree-ring based climate reconstructions (Briffa et al., 1998; D'Arrigo et al., 2014, 2008). DP has been reported from regions thousands of kilometers apart in Alaska (Barber et al., 2000), Western Siberia (Kirdyanov et al., 2020), and Tibet (Zhang et al., 2018) whereas it has been less prevalent or non-existent at other sites such as in the European Alps (Büntgen et al., 2008). Various reasons for DP have been proposed including drought stress (Barber et al., 2000; D'Arrigo et al., 2004), "global dimming" resulting from reduced solar radiation in high latitudes caused by human activity (Stanhill and Cohen, 2001), or pollution (Kirdyanov et al., 2020; Rydval and Wilson, 2012) as well as methodological issues (Allen et al., 2018; Esper et al., 2005; Loehle, 2009) and instrumental data uncertainties (Frank et al., 2007) Assessments of DP are complicated as different assumptions and decisions can be made during data treatment (Büntgen et al., 2021a; Esper and Frank, 2009). DP can be defined (D'Arrigo et al., 2008) as both a deviation in trend and/or a weakening of high-frequency covariance between instrumental and proxy data, two phenomena that may not be mutually exclusive (Büntgen et al., 2009).

An extensive amount of tree-ring width (TRW) data exists across the

* Corresponding author.
E-mail address: mkunz01@uni-mainz.de (M. Kunz).

https://doi.org/10.1016/j.dendro.2025.126399
Received 31 March 2025; Received in revised form 19 August 2025; Accepted 25 August 2025
Available online 26 August 2025
1125-7865/© 2025 The Authors. Published by Elsevier GmbH. This is an open access article under the CC BY license (http://creativecommons.org/licenses/by/4.0/).

northern and elevational tree line, allowing for regional estimates of DP. However, records based on maximum latewood density (MXD) (Björklund et al., 2019; Schweingruber et al., 1979) as the superior temperature proxy used in most robust temperature reconstructions (Briffa et al., 2001; D'Arrigo et al., 2014; Esper et al., 2020, 2016; Schweingruber and Briffa, 1996) are much sparser. In recent years, latewood blue intensity (LWBI) has been established as a more cost-effective surrogate for MXD (Kaczka and Wilson, 2021; McCarroll et al., 2002; Rydval et al., 2014; Wilson et al., 2019). Additionally, the Delta blue intensity parameter representing the difference between maximum earlywood and minimum latewood BI has been explored to mitigate potential low-frequency biases in raw LWBI data resulting from color changes of the wood surface (Björklund et al., 2014; Fuentes et al., 2018; Reid and Wilson, 2020). One of the earliest observations of DP was made in the Alaskan portion of north-west North America (NWNA) (Jacoby and D'Arrigo, 1995) with more recent research confirming divergence for large parts of the region (Barber et al., 2000; Driscoll et al., 2005; Lloyd and Fastie, 2002; Porter and Pisaric, 2011; Wilmking and Singh, 2008). In the neighboring Yukon Territory (YT), the Twisted-Tree Heartrot Hill site was used for one of the first temperature reconstructions from NWNA (Jacoby and Cook, 1981), which has served as a striking example of a positive association between tree growth and temperature not only becoming weaker but even significantly negative in the second half of the 20th century. This has been related to temperature exceeding a threshold beyond which it is replaced by precipitation as the primary factor limiting radial tree growth (D'Arrigo et al., 2004), an assumption which was already made for Alaska by Jacoby and D'Arrigo (1995). Subsequent studies in the YT found more stable climate-growth relationships in 1) MXD (Morimoto, 2015) and LWBI (Reid et al., 2025; Wilson et al., 2019) than TRW and 2) in the southern compared to the northern part of the region (Morimoto, 2015; Youngblut and Luckman, 2008). While the stronger performance of the density-based records is not surprising considering the lower impacts of memory effects on these proxies and their higher skill in replicating annual temperature variability (Esper et al., 2015), straightforward causes for different expressions of DP on a rather small spatial scale have yet to be identified.

Here, we aim to better quantify DP and its drivers by analyzing various factors that may cause shifts in both long-term trends and interannual coherence between instrumental temperatures and tree-ring (TR) data. While we address this differentiation whenever feasible, we acknowledge that the combination of these two sources may affect any tree-ring chronology and may not always be statistically separable. To first assess potential disparities between TR proxies, we present new TRW, LWBI, and MXD data from two white spruce (*Picea glauca*, Moench Voss.) sites across the YT, one site in the south (Canyon Lake, CNY) and one from the north (North Klondike River, NKL, Fig. 1a). As MXD and LWBI essentially measure similar wood properties (Björklund et al., 2024, 2014), we compare respective measurements from the same trees and quantify differences regarding their climate signal and trends. White spruce is ideal for such a comparison as color changes between heartwood and sapwood, which would affect LWBI values, are typically negligible in this species (Björklund et al., 2015; Reid et al., 2025; Wilson et al., 2019, 2017). Furthermore, we incorporate more MXD samples of different tree age classes to assess potential biases resulting from lower replication or age effects and allow data pruning as a simplified version of age-band decompositioning, a technique that may help preserve low-frequency variability (Briffa et al., 2001; Homfeld et al., 2024). Various detrending methods are tested to evaluate their effect on the magnitude of divergence estimates. A decoupling with the TR proxy records may also result if the instrumental data are not reliable. Thus, we also consider differences between two widely used gridded datasets and identify inconsistencies in the underlying station records. Since regional differences in diurnal temperature ranges and their trends have been observed in previous research (Zhong et al., 2023), we additionally evaluate DP by comparing maximum and minimum temperature with our TR data. Applying several statistical metrics, we systematically assess the effect of each of these potential drivers of DP in the YT considering shifts both in trend and interannual coherence.

2. Material and methods

2.1. Site characteristics

Core samples were collected in July of 2022 in the context of a larger sampling campaign, updating and extending a TRW and LWBI network in the southern and central YT (Reid et al., 2025; Wilson et al., 2019; Youngblut and Luckman, 2008). Both sites are mixed-age white spruce stands close to elevational tree line. NKL is located in central YT at 64.44° N and 138.26° W at 990 m a.s.l. within the valley of the North Klondike River as part of the Ogilvie Mountains (Fig. 1a). Annual mean temperature of the area is −7.8 °C and annual mean precipitation is 345 mm (Fig. 1b; 1961–1990, Harris et al., 2020). CNY is located on a western slope near the eastern shore of Canyon Lake at 61.12° N and

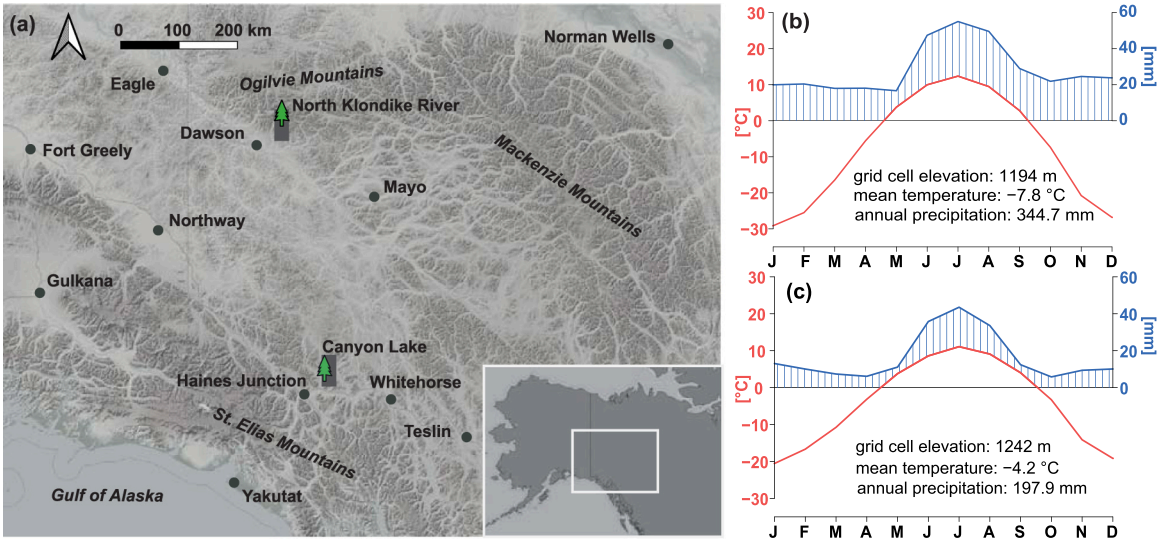

Fig. 1. Map showing the locations of study sites (trees), CRU TS 4.08 grid cells used for climate diagrams (grey rectangles) and climate stations (black dots) in the YT region (a). Climate diagrams for NKL (b) and CNY (c) tree sites show mean values from 1961–1990.

136.99° W and 1100 m a.s.l. in the southern YT. The difference in site elevation reflects the latitudinal impact on local temperatures lowering tree line towards the north. The mean annual temperature is −4.2 °C and precipitation 198 mm. The climate of both regions is characterized by large differences in mean temperature of more than 30 (CNY) or even 40 °C (NKL) between the coldest (January) and the warmest (July) month. Located on the leeward side of the St. Elias Mountains, the highest mountain range in Canada reaching almost 6000 m a.s.l., the southern part of the YT is particularly dry. Summer is much wetter than all other seasons with more than half of annual precipitation at both sites falling between June and September. All other months barely exceed 20 (NKL) or even 10 mm (CNY) causing a critical water deficit during the early growing season (Jätzold, 2000) and making the region's forests susceptible to drought stress related to climate change (Reid et al., 2022).

2.2. Sampling, measurements, and data treatment

One hundred TRW/MXD cores (2 each from 50 trees) and 31 LWBI cores (1 each from 31 trees) were sampled at each site with all three parameters being available from 25 (NKL) and 17 (CNY) trees. Whereas LWBI samples were only taken from mature trees, cores used for TRW and MXD aimed to represent a balanced age structure including young and old individuals. TRW data were measured using LINTAB 6 devices (Rinntech, Germany) and TSAP software (Rinn, 2003). To account for changes in fiber angle, each sample wascut into 2–4 cm long, and 1.2 mm thin sections orthogonal to the tracheids' longitudinal axis. After x-raying, brightness of the resulting images was recorded at a resolution of 0.01 mm using a DENDRO2003 X-ray microdensitometer (WALESCH Electronic GmbH, Switzerland) as described in Björklund et al. (2019) and resulting MXD values were extracted. For LWBI, after being sanded to 1000 grit, samples were scanned at 3200 dpi using an Epson V850 pro scanner and SilverFast software. LWBI data were obtained in CooRecorder software (Cybis Elektronik and Data AB, Sweden). All measurements were crossdated using TSAP (TRW, MXD) and CDendro (LWBI) (Cybis Elektronik and Data AB, Sweden) software, with final validation using Cofecha (Holmes, 1983). To evaluate the effect of detrending choice on climate signals, several methods were performed in ARSTAN (Cook, 1985; Cook et al., 2017a) and RCSsigFree (Cook et al., 2017b) programs including a negative-exponential curve (NegEx), a simple age-dependent spline (ADS, (Melvin et al., 2007)), and an ADS within the signal-free framework (SF), constraining a positive slope of the spline. The objective of SF is to account for trend distortion biases due to climate forcing by removing these common signals from raw series before iteratively estimating the detrending curve (Homfeld et al., 2024; Melvin and Briffa, 2014, 2008). In addition, raw MXD series were pruned to a window of equal biological age to suit the regional curve standardization (RCS) detrending approach (Briffa et al., 1992; Cook et al., 1995; Esper et al., 2003) which aims to mitigate biases introduced by age effects in TR data (Esper et al., 2016) and may be a promising approach to address this potential driver of DP (Briffa et al., 2001; Homfeld et al., 2024; Römer et al., 2021). The time span between 31 and 120 years was found to avoid distortions caused by juvenile growth while maintaining a minimum replication of over 20 series since at least 1900. In addition to classic RCS, the pruned datasets were subsequently detrended using the SF RCS variant that has seen increasing popularity in recent years and is designed to combine the advantages of SF and RCS aiming to preserve a maximum amount of potential temperature variance (Homfeld et al., 2024; Shi et al., 2020; Zhang et al., 2016).

2.3. Climate-growth relationship and divergence assessment

Since the selection of the instrumental calibration target can have a significant impact on proxy-based climate reconstructions (Frank et al., 2007), we used mean (Tmean), maximum (Tmax), and minimum temperature (Tmin) data from the closest single grid cells from both sites (Tab. S1) of the gridded Berkeley Earth Surface Temperature (BEST, Rohde and Hausfather, 2020) and Climate Research Unit (CRU, version 4.08, Harris et al., 2020) products while also considering information from individual stations. To investigate potential effects of limited water availability, CRU TS precipitation and self-calibrated Palmer Drought Severity Index (scPDSI, Wells et al., 2004) were used. For the common period of 121 years (1901–2021), we divided the interval into two halves. TR chronologies were scaled (Esper et al., 2005) to instrumental data of the first half (1901–1960) by adjusting their means and standard deviations accordingly to display and emphasize any potential non-stationary responses in the second half (1961–2021). Strength and stability of the relationship between instrumental and proxy data were determined using several metrics. These include the range of scaled TR chronologies in °C to illustrate the amount of temperature variation captured. Root-mean-squared deviations and linear regression slopes of residuals between proxy and target were calculated to assess both the overall difference between the two respective timeseries and its trend serving as a measure of low-frequency divergence. Bootstrapped stationary and 31-year moving window correlations function as measures of strength of climate-growth relationships and their change over time. Analyses were conducted using R version 4.3.2. (R Core Team, 2023) as well as "dplR" (Bunn, 2008), "treeclim" (Zang and Biondi, 2015), and "dendroTools" (Jevšenak and Levanič, 2018) packages.

3. Results

3.1. Tree-ring parameter comparison

We present new TRW and MXD measurements from 100 living white spruce trees from two sites, both of which are at least 200 years old. These partially overlap with two sites sampled for the Yukon LWBI network (Reid et al., 2025). All three tree-ring parameters were measured from a subset of 25 (NKL) and 17 (CNY) trees. Despite the limited sample replication in these comparisons, EPS values for all proxies exceed the accepted common signal threshold of 0.85 (Table 1, Wigley et al., 1984) prior to 1901, marking the beginning of our climate-growth analysis period. In accordance with prior research, first-order autocorrelation (AR1) and rbar are higher for TRW compared with MXD and LWBI at both sites. However, there are also differences between the two wood density-based proxies, with LWBI showing a higher AR1 (0.73 (NKL) and 0.69 (CNY) vs. 0.45 and 0.35) and similarly a higher rbar (0.46 and 0.56 vs. 0.19 and 0.33) than MXD. After detrending (ADS), LWBI retains a higher AR1 across both sites (0.39 and 0.30 vs. 0.31 and 0.20), however, rbar is identical at NKL and even slightly higher for MXD at CNY (Table 1). This is also reflected in the raw (Fig. S1a) and age-aligned mean curves (Fig. S1b) of both sites with LWBI, similarly to TRW, showing a marked decline with time and age. Conversely, MXD values decline less over time and show greater interannual variability, especially at NKL. Given these growth trends, ADS detrending was found suitable for initial comparisons. Tmax has been deemed the optimal calibration parameter for MXD and LWBI records from Western North America in numerous studies (Heeter et al., 2021; King et al., 2024; Reid et al., 2025; Seftigen et al., 2022; Wilson et al., 2019), which is confirmed here with our sites showing higher correlations compared with Tmean across proxies and periods (Figs. S2–5). These results were stronger when using BEST rather than CRU data for both sites and in almost all months and seasons. Accordingly, BEST Tmax data were used for most of the following analysis.

Correlations between TRW and Tmax are negative for both sites (Fig. S6, r = -0.37 at NKL and −0.33 at CNY, $p < 0.05$) for previous summer (JJA) and weakly positive (CNY) or insignificant (NKL) for current summer (Fig. 2). In contrast, MXD chronologies derived from the common subset series are strongly correlated with temperature (1901–2021) peaking in July at NKL and in August at CNY (Fig. 2a, c, r = 0.57 for both sites). Results for seasonal May–August (MJJA) temperatures are similarly robust (NKL r = 0.63, CNY r = 0.61), with 31-year moving correlations for this season remaining significant

Table 1
Descriptive statistics of TR datasets including sample replication (Rep.), mean segment length (MSL), first-order autocorrelation (AR1), interseries correlation (Rbar), and expressed population signal (EPS) for raw and age-dependent spline detrended series.

NKL	Proxy	Period	Rep.	MSL	AR1 raw	Rbar raw	EPS raw	AR1 ADS	Rbar ADS	EPS ADS
common subset	TRW	1793–2021	25	158	0.85	0.70	0.98	0.55	0.35	0.93
	MXD	1795–2021	25	155	0.45	0.19	0.86	0.31	0.24	0.89
	BI	1793–2021	25	156	0.73	0.46	0.95	0.39	0.24	0.89
all samples	TRW	1793–2021	100	125	0.80	0.36	0.98	0.55	0.27	0.97
	MXD	1795–2021	100	118	0.41	0.20	0.96	0.27	0.23	0.97
	BI	1772–2021	31	162	0.75	0.50	0.97	0.38	0.23	0.90
CNY	**Proxy**	**Period**	**Rep.**	**MSL**	**AR1 raw**	**Rbar raw**	**EPS raw**	**AR1 ADS**	**Rbar ADS**	**EPS ADS**
common subset	TRW	1833–2021	17	160	0.77	0.48	0.94	0.46	0.46	0.93
	MXD	1835–2021	17	155	0.35	0.33	0.89	0.20	0.35	0.90
	BI	1825–2021	17	155	0.69	0.56	0.96	0.30	0.28	0.87
all samples	TRW	1822–2021	100	130	0.72	0.35	0.98	0.46	0.37	0.98
	MXD	1820–2021	100	120	0.37	0.26	0.97	0.25	0.30	0.98
	BI	1825–2021	31	159	0.72	0.60	0.98	0.31	0.28	0.92

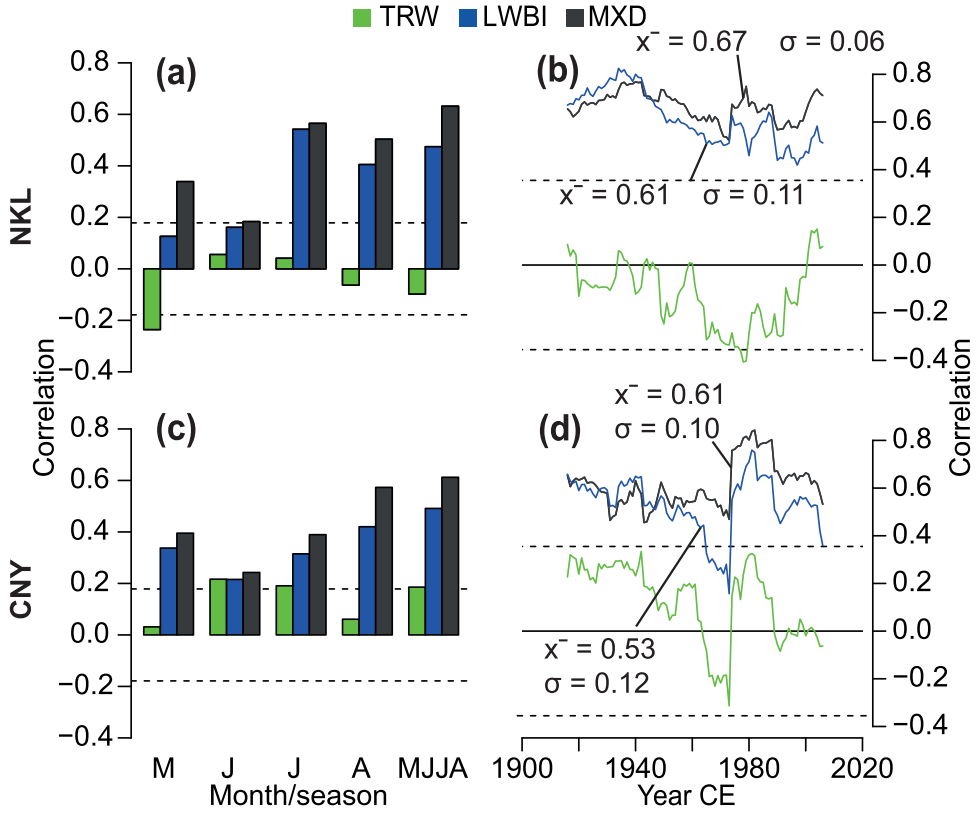

Fig. 2. Pearson correlation coefficients for NKL **(a, b)** and CNY **(c, d)** TR proxies and monthly and seasonal BEST Tmax **(a, c)** over the full calibration period from 1901–2021 and **(b, d)** 31-year moving windows considering May–August temperatures. Dashed lines are significance thresholds for $p < 0.05$. Numbers are arithmetic means ($\bar{x}$) and standard deviations (σ) of moving-correlation coefficients and dashed lines are $p < 0.05$ significance thresholds.

($p < 0.05$) throughout the entire period. LWBI correlation values, while also significant for July, August, and MJJA, are consistently weaker (MJJA: NKL r = 0.47, CNY r = 0.49) and moving windows reveal that this gap between MXD and LWBI opened in the 1950s after both proxies exhibited similar correlations during the first half of the 20th century (Fig. 2b, d). This is particularly evident at CNY where LWBI correlations sharply decrease between 1950 and 1970, becoming insignificant for over a decade, which corresponds to a marked decline in TRW correlations. Differences between MXD and LWBI are reduced when June–August (JJA) instead of MJJA temperatures are used but MXD results generally remain stronger, especially for CNY (Figs. S2–5). Since MXD and LWBI correlations are overall higher with MJJA than JJA, except for NKL LWBI in the first half (1901–1960) of the investigated period, MJJA was utilized for all further comparisons.

Scaling the chronologies to instrumental data of the 1901–1960 period to highlight trend divergence (Fig. 3) indicates a notable offset between MXD or LWBI and temperature after the 1970s (CNY; Fig. 3e, f) or 1980s (NKL; Fig. 3b, c). This divergence is stronger for LWBI at both sites, indicated by higher root-mean squared deviation (RMSD) between proxy and temperature and lower total change (TC) values of corresponding residual trends. Following declines in MXD and LWBI values in the 1990s and early 2000s at both sites, both proxies began to recover in recent years narrowing the gap with instrumental temperature. First-differencing MXD, LWBI, and temperature time series to remove any lower-frequency trends strongly reduces RMSD differences for both sites and moving correlation differences for NKL between the two tree-ring proxies (Fig. S7). However, correlations are still higher and more stable with MXD for CNY. Given that MXD outperforms LWBI across all metrics, we focus on this parameter for subsequent analyses.

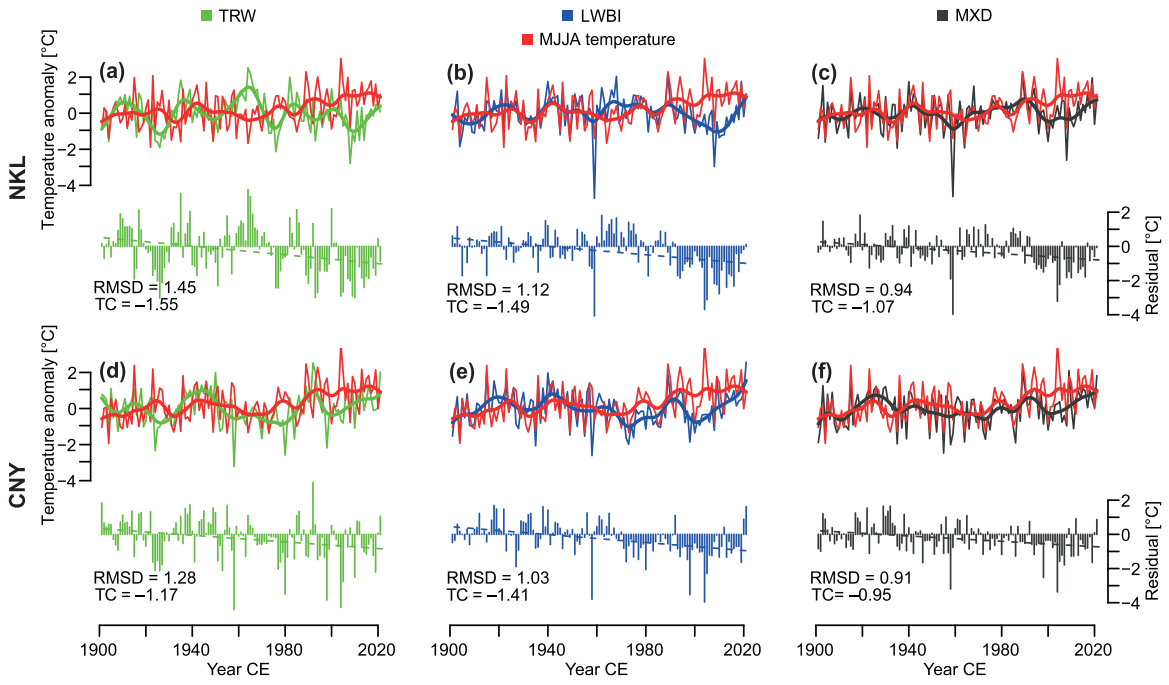

Fig. 3. Scaled (1901–1960) TRW, MXD and BI chronologies from NKL **(a–c)** and CNY **(d–f)** shown together with BEST May–August Tmax anomalies from 1901–1960 (thin curves) and 15-year low-pass filters (bold curves). Bar plots show annual residuals between TR and instrumental data with numbers denoting root-mean square deviations in °C (RMSD) and total changes (TC) derived from linear regressions (dashed lines) from 1901–2021. Residuals were calculated by subtracting instrumental from proxy temperatures.

3.2. Detrending method comparison

Utilizing the highly replicated MXD dataset of mixed-age trees instead of the common subset used for the proxy comparison slightly increases correlation with MJJA Tmax when again applying ADS detrending (NKL r = 0.66, CNY r = 0.67, Fig. 4c, g). Incorporating four additional detrending methods yields only minor variations in both trend and correlation. However, SF ADS produces the strongest results

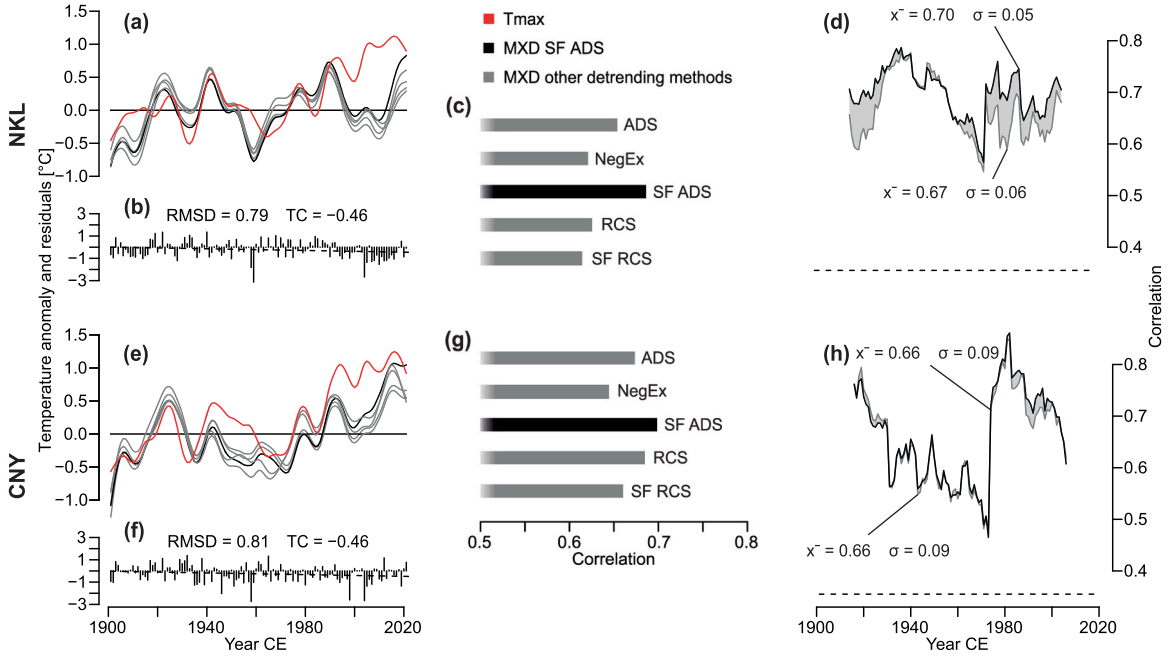

Fig. 4. 15-year low-pass filters of scaled (1901–1960) MXD chronologies for five detrending methods shown together with BEST May–August Tmax anomalies **(a, e)**. Corresponding bar plots **(b, f)** show annual residuals between the detrending version (SF ADS = signal-free age-dependent spline) with the lowest root-mean square deviation (RMSD) and instrumental data. Numbers denote RMSD in °C and total changes (TC) from linear regression (dashed lines) from 1901– 2021. Grey and black bars **(c,g)** are Pearson correlations with Tmax (1901–2021) for five detrending methods (ADS = age-dependent spline, NegEx = negative exponential function, SF ADS, RCS = regional curve standardization, SF RCS = signal-free RCS). **(d)** and **(h)** show 31-year moving-window correlations with Tmax for detrending methods with the highest (SF ADS) and lowest (NegEx) full-period correlations as shown in **(c)** and **(g)**. Numbers are arithmetic means ($\bar{x}$) and standard deviations (σ) of moving-correlation coefficients and dashed lines are $p < 0.05$ significance thresholds. Upper panel shows results for NKL, lower panel for CNY.

across all metrics indicated by lower RMSD, less negative TC (Fig. 4b, f), and higher correlations with instrumental temperature at both sites (Fig. 4c, g). SF RCS (NKL) as one of the methods utilizing the pruned datasets and NegEx (CNY) show the weakest correlation results. Differences in moving correlation patterns between the detrending methods are again rather minor and primarily occur in the NKL data (Fig. 4d) during the period of strongest trend mismatch between proxy and instrumental temperature from the 1980s to the 2000s (Fig. 4a).

3.3. Instrumental target comparison

Both BEST and CRU gridded datasets display a long-term warming trend across the Yukon that accelerates in the second half of the investigated period (Fig. 5a, e, Fig. S8). However, they repeatedly show trend offsets on shorter timescales, with the CRU dataset reporting warmer maximum temperatures during the 1900s and 1910s and BEST showing a faster increase in recent decades, especially at CNY. Annual residuals between BEST and CRU repeatedly exceed 0.5 °C after 1990 and show a distinct positive trend, indicating that the gap between the two datasets has been widening (Fig. 5e, f). According to BEST, 2004 is the warmest May–August period for both NKL and CNY, while CRU reports 1989 as warmer at CNY (Fig. S8). MXD aligns more closely with the BEST data for NKL resulting in a lower RMSD, however, due to stronger BEST warming since the 1960s at CNY, RMSD is lower for CRU at this site. Still, MXD correlations are higher with BEST than CRU Tmax at both sites (NKL: 0.69 vs. 0.61, CNY: 0.70 vs. 0.64, Fig. 5c, g). Moving-window correlations are also continuously higher and more stable with BEST which is particularly evident at NKL between the 1940s and 1970s (Fig. 5d, h), a period centered around a striking low-density anomaly in 1959 more than four standard deviations below the chronology mean.

Long-term trends of temperature variables are overall consistent between the two sites (Fig. 6). Tmean and Tmax anomalies range between 0.5 and –0.5 °C until the middle of the 20th century before rapidly rising from the 1960s to the 1990s and stabilizing around 1 °C since the 2000s. Conversely, minimum temperatures are constantly increasing throughout the entire period, creating a gap of temporarily over 0.8 °C between Tmax and Tmin anomalies from the 1940s to the 1980s (Fig. 6a, e). Trends of Tmin and MXD decouple during this period with the MXD chronology reaching a low point while Tmin is rising. Consequently, correlations with Tmin are notably weaker for all metrics for the whole period (NKL 0.50, CNY 0.49; Fig. 6c, g) and demonstrate less stability over time (Fig. 6d, h). Tmean produces stronger results than Tmin across all metrics but is still slightly weaker than Tmax with full-period correlations reaching 0.62 (Tmax: 0.69) at NKL and 0.66 (Tmax: 0.70) at CNY.

3.4. Comparing impacts of methodological choices on trend divergence and correlation

Choosing MXD instead of TRW and LWBI provides the clearest improvement across all metrics representing trend divergence (TC), interannual coherence (strength and stability of correlations) or both (RMSD) (Figs. 2, 3). When comparing the influence of varying detrending methods, instrumental datasets, and diurnal temperature variables (Fig. 7), temperature variables show the most significant differences in most cases. Tmax yields the largest temperature range captured by the chronology, the flattest residual slope as a measure of trend divergence, and the highest and most stable correlations with MXD, while Tmin produces the weakest and Tmean intermediate results. However, Tmean outperforms Tmax in terms of RMSD at both sites. Among the two gridded products, BEST shows stronger correlation statistics at both sites, yet RMSD at CNY is smaller for CRU, likely due to the weaker temperature increase inherent in this dataset reducing divergence in trend for the most recent decades. Similarly, residual slopes are less negative for CRU, even creating a positive trend at CNY (Fig. 7h). The different detrending approaches result in similar variability at both sites with SF ADS largely outperforming the four other methods across all metrics. Overall, the most pronounced absolute differences between the two sampling sites are observed in temperature range (Fig. 7a, f) and moving correlation stability (Fig. 7e, j), both of which are higher at NKL than CNY.

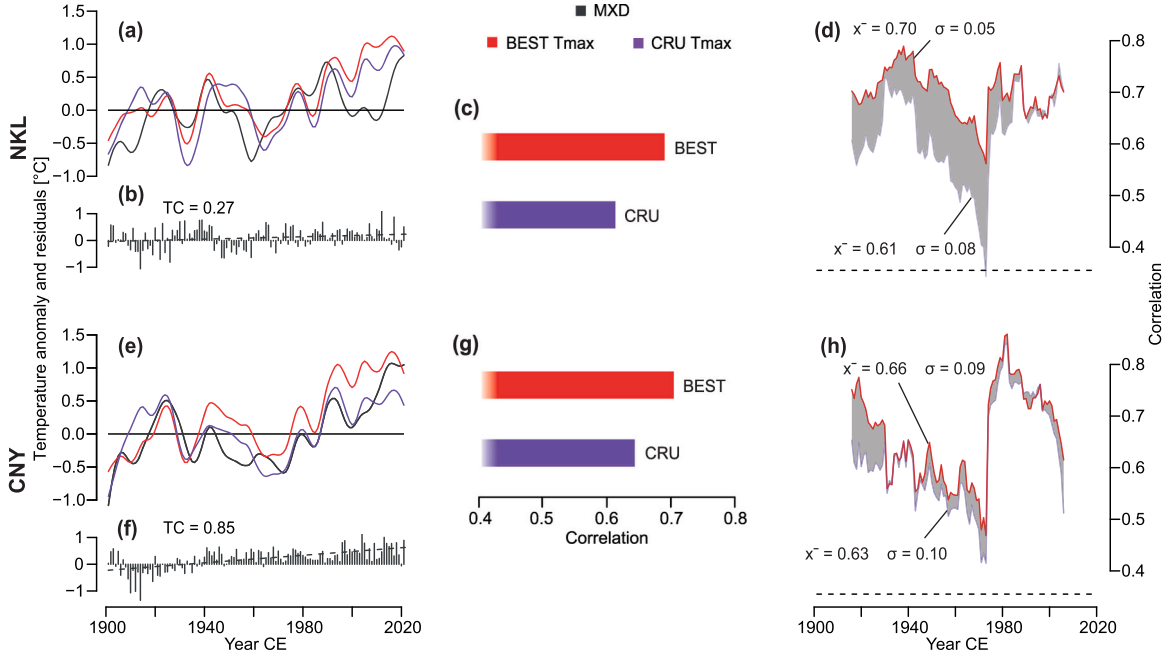

Fig. 5. 15-year low-pass filters of scaled (1901–1960) SF ADS (signal-free age-dependent spline) MXD chronologies shown together with target BEST and CRU TS May–August Tmax anomalies (a, e). Corresponding bar plots (b, f) show annual differences between BEST and CRU Tmax. Numbers denote total changes (TC) from linear regression (dashed lines) from 1901–2021. Bars (c, g) are Pearson correlations against Tmax (1901–2021). (d) and (h) show 31-year moving-window correlations with Tmax with numbers indicating arithmetic means ($\bar{x}$) and standard deviations (σ) of running coefficients and dashed lines $p < 0.05$ significance levels. Upper panel shows results for NKL, lower panel for CNY.

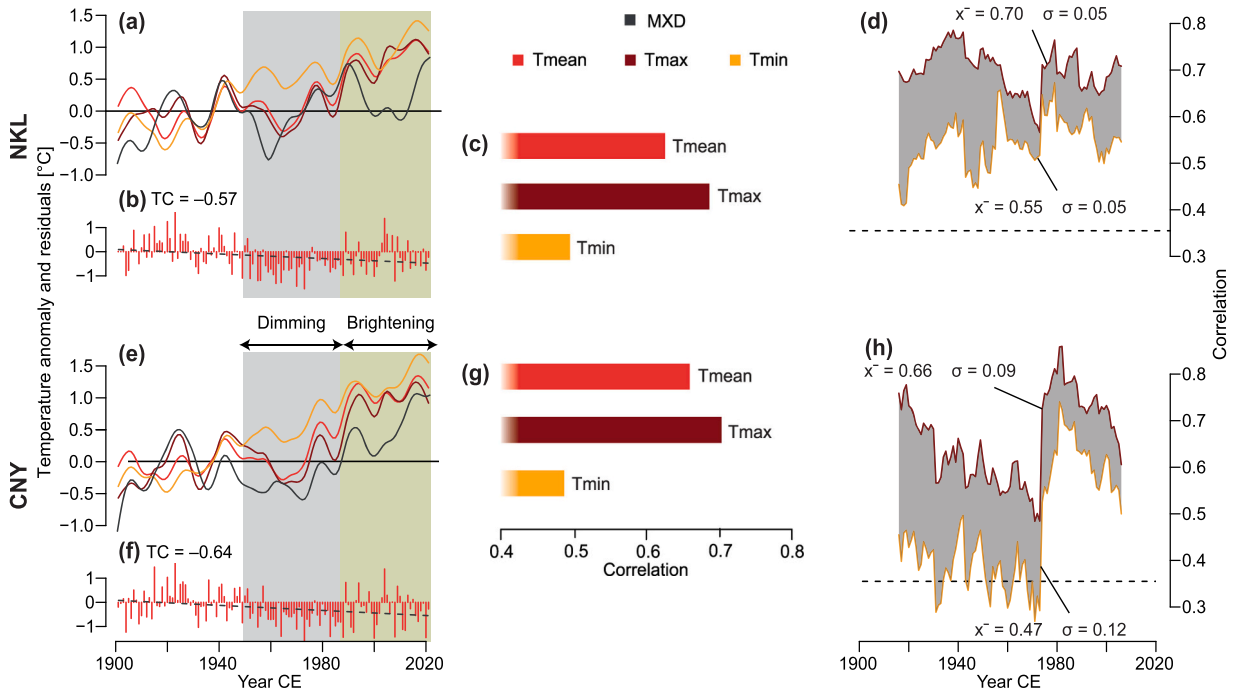

Fig. 6. 15-year low-pass filters of scaled (1901–1960) SF ADS (signal-free age-dependent spline) MXD chronologies shown together with BEST May–August Tmean, Tmax, and Tmin anomalies (a, e). Corresponding bar plots (b, f) show annual differences between Tmax and Tmin anomalies. Numbers denote total changes (TC) from linear regressions (dashed lines) from 1901–2021. Bars (c, g) are Pearson correlations with mean, maximum, and minimum temperatures (1901–2021). (d) and (h) show 31-year moving-window correlations against maximum and minimum temperature numbers indicating arithmetic means ($\bar{x}$) and standard deviations (σ) of moving-correlation coefficients and dashed lines significance thresholds. Upper panel shows results for NKL, lower panel for CNY. Grey and yellow s hadings in **a, b, e,** and **f** are global dimming and brightening periods as shown in Wild (2009).

4. Discussion

4.1. Differences between tree-ring parameters

Weak results for TRW in residual and correlation analyses (Figs. 2, 3, and S6) demonstrate that there is no simple linear relationship between this proxy and temperature at our two sites, suggesting that it is limited by different climatic factors varying from year to year. At the drier CNY site, TRW is temporarily positively correlated with accumulated precipitation (Fig. S9a, c) and scPDSI (Fig. S9b, d) from previous fall to current summer indicating water availability as an additional growth-limiting factor at least during early growing season (Chavardès et al., 2013). Surprisingly, Youngblut and Luckman (2008) found highly significant positive correlations with early summer temperature in TRW from a site near our CNY at an elevation 100 m lower, whereas in our data, the relationship with temperature is weak and unstable. NKL TRW was previously correlated with scPDSI and precipitation but here the relationship became insignificant after the 1980s. Thickness and duration of snow cover insulating trees from severe frost events may additionally affect growth and thus climate signals, especially in the northern YT (Griesbauer and Green, 2012). This interaction mainly concerns conditions during the early growing season throughout which the earlywood, making up the majority of TRW, is formed (Cuny et al., 2014; Glock, 1937; Higuchi, 1997).

Conversely, the two latewood-based proxies appear less influenced by other climate parameters. While both significantly correlate with MJJA temperature, LWBI consistently underperforms compared to MXD at both sites. Using a different season (JJA) does improve the LWBI results of one site (NKL), but MXD correlations remain higher (Fig. S2, S3). Although potential discoloration issues may be one reason for long-term distortions in trend (Wilson et al., 2021, 2017), they do not explain lower and less stable running correlations of LWBI, which indicate a weaker representation of high-frequency temperature variability in this proxy. Such an effect may be caused by measurement resolution being too low to adequately represent the wood properties, that are most closely linked with summer temperature (Babst et al., 2009). This issue may be more prevalent in LWBI than MXD measurements (Seftigen et al., 2022) and aggravated in sections of very narrow rings (Björklund et al., 2019). Hence, the negative trend in TRW of both sites may have biased the corresponding LWBI measurements towards lower values (Fig. S1), both increasing trend divergence for this proxy and weakening its potential to capture positive temperature anomalies during single years. Although the MXD chronologies appear to be less affected by such distortions, they still fail to fully track the instrumental warming trend. This may be related to extremely warm summers such as 2004 crossing a threshold beyond which tree growth response to temperature declines (D'Arrigo et al., 2004; Reid et al., 2025).

4.2. Effects of detrending and data pruning

Focusing on a smaller sample size of dominant and/or mature trees is a common and sensible practice in dendroclimatic calibration as it provides the maximum amount of information for minimum time and effort (Fritts, 1971). However, this practice may decrease representativeness when reconstructing climatic variables, as the strength of climate-growth relationships may change with cambial age (Esper et al., 2008; Konter et al., 2016). Replacing the mature-tree MXD subset used for the proxy comparison (Figs. 2, 3) with the full mixed-age dataset of 100 samples introduced in the detrending comparison (Fig. 4) already leads to higher correlations with temperature when applying the same detrending method (ADS). This enhancement is expected as a higher sample replication tends to increase the common signal as shown in Table 1 (Fritts, 1976; McPartland et al., 2024; Speer, 2010). As DP is partially a problem of deviating low-frequency trends (D'Arrigo et al., 2008), choosing an appropriate detrending method can be critical. However, the differences between the five approaches tested here are relatively minor for both sites (Figs. 4 and 7), likely due to weak mid- and low-frequency variability in the MXD raw data, especially compared

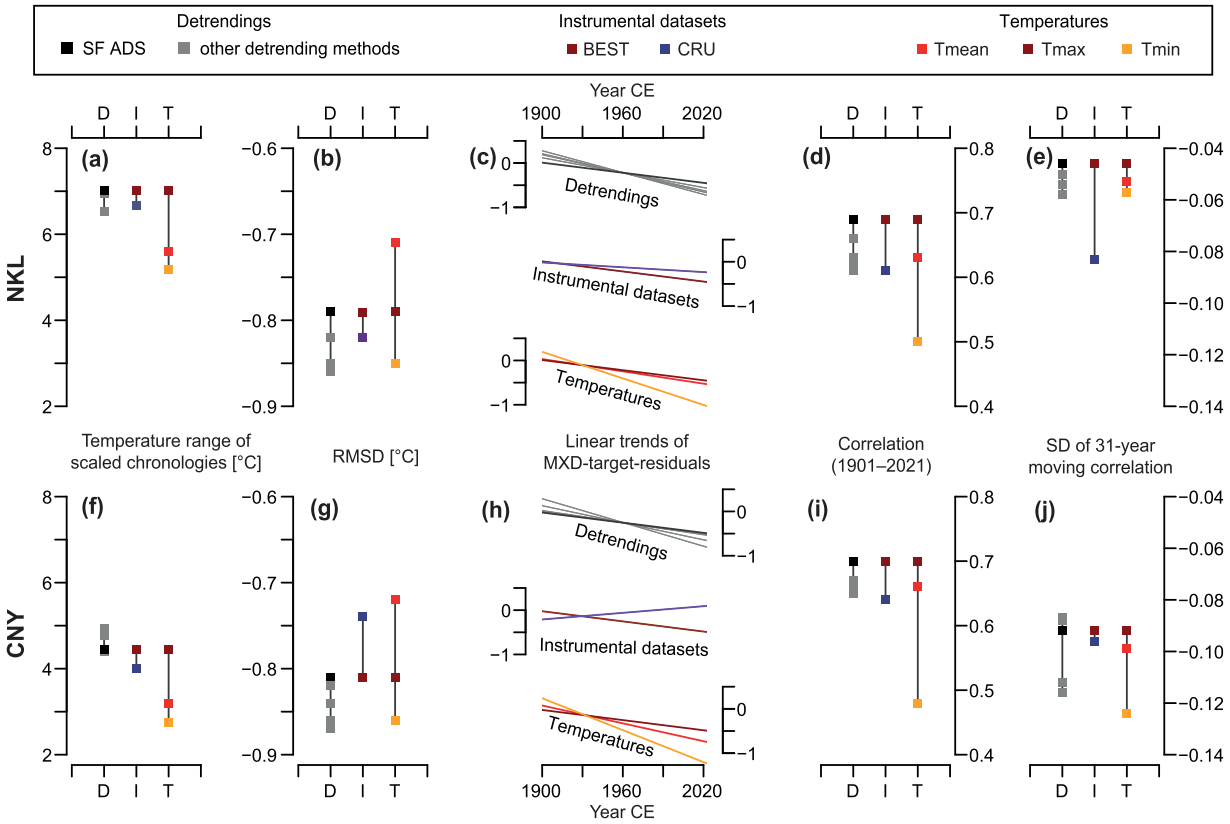

Fig. 7. Metrics evaluating differences between MXD chronologies based on varying detrending methods (D), instrumental datasets (I), and temperature variables (T) including: range of scaled chronologies as the difference between the highest and lowest value (a, f), additive inverse root-mean-squared deviation between MXD and target temperature (b, g), linear trends in residuals between MXD and target (c, h), Pearson correlations for the full period (1901–2021) (d, i), and standard deviations of 31-year moving correlations (e, j). Upper panel shows results for NKL, lower panel for CNY.

to TRW or LWBI data from the same trees (Fig. S1). However, the SF ADS chronologies best track the instrumental upward trend in recent decades at both sites, albeit still falling short of the instrumental temperature increase. The method has been shown to preserve mid- to low-frequency trends that may be removed by other detrending techniques, accounting for the naturally changing patterns of tree growth with increasing age (Wilson et al., 2019). This finding agrees with studies that applied SF ADS to LWBI datasets from the same region (Reid et al., 2025; Wilson et al., 2019) and a larger area across Western North America (Heeter et al., 2021). In contrast, NegEx, which does not address such variance changes, provides the flattest reconstructions. Regarding the pruned datasets, the RCS version temporarily tracks the instrumental warming more closely than the other methods. However, correlations with Tmax are weakened compared to SF ADS, possibly due to reduced sample replication and thus EPS, especially towards the end of the 20th century (Fig. S10). Consequently, while pruning and RCS may help mitigate trend divergence, their potential to capture high-frequency variation appears to be limited. These observations highlight the difficulty of obtaining a suitable TR dataset for RCS, even if a comparatively large number of trees of different ages are sampled. Combining measurements from several sites growing under similar climate conditions or separately treating high- and low-frequency components of TR chronologies may help resolve this issue.

4.3. *Effects of instrumental target selection*

In the sparsely populated YT, gridded climate datasets like the BEST and CRU products rely on a very limited number of single records that each strongly affect the resulting gridded data while also including distant stations that potentially dilute a subregional signal. Small-scale weather events may have been recorded by TR proxies but missed by widely dispersed instrumental stations (Mankin et al., 2024). Such a subregional anomaly occurred in late summer of 1959 causing a ring of exceptionally low density at NKL, which has also been observed in several other sites across NWNA (Leland et al., 2025). As the most prominent negative temperature deviation during this event was recorded by the Dawson and Mayo stations, it seems to have been confined to the northeastern part of the region (Fig. S11). A brief but intense cold spell in early August including several frosty nights in Dawson (Menne et al., 2018) at an elevation more than 600 m lower than the NKL site location prematurely ended latewood formation, while stations further southwest recorded temperatures close to or above the mean. Consequently, correlations of NKL MXD during the period surrounding 1959 are by far the highest with the Dawson, Mayo, and Eagle records (Fig. S12), all of which start early in the 20th century. Stations further southwest (e.g. Northway, Haines Junction, and Whitehorse), which correlate lower, were established during Alaska Highway construction in the early 1940s (Coates and Morrison, 2015; Harris et al., 2020; Lawrimore et al., 2011). Dawson is only 56 km from the NKL site and the BEST interpolation, which emphasizes stations sharing common variability (Rohde and Hausfather, 2020), appears to put more weight on this record than the Angular Distance Weighting used for the CRU data (Harris et al., 2020). CRU is likely to be impacted by the higher number of stations further south unaffected by the cold spell, providing MJJA values 0.6 °C higher than BEST. Moving-window correlations with the CRU data drop markedly compared to BEST but also the Dawson and Mayo stations (Fig. S11). Hence, the number of stations available is not a measure of the representativeness of the resulting gridded data or its usability for dendroclimatic calibration and the period of highest instrumental station density from 1948 to 1974 paradoxically coincides with reduced coherence between MXD and gridded temperatures. Spearman's rank correlation coefficient, which is typically lower,

exceeds Pearson's r during this time span (Fig. S13), underlining the significance of the 1959 ring.

Including the Alaska Highway stations appears to contribute to declining coherence between gridded temperatures and MXD beyond just the 1959 event. Despite no similar evidence of the 1959 cold, correlations of CNY with Mayo and Dawson are again notably higher than with Haines Junction which is much closer and presumably exerts a more substantial impact on the gridded products (Fig. S14). While all these observations suggest the Dawson and Mayo stations as optimal calibration targets, BEST gridded data still seem more suitable as Dawson correlations with the southern site are less stable (Fig. S10) and the Mayo record is shorter (1925–1990), missing the last 30 years (Lawrimore et al., 2011). Reid et al.'s (2025) analysis found that BEST performed better in the early and CRU in the later part of the period (1901–2021), albeit with a different CRU version (4.07). In our analysis focusing on two MXD sites, correlation results with BEST are slightly higher for the most recent period. The warming trend in CRU Tmax has remarkably muted since the 1990s resulting in smaller residuals of CNY with CRU than with BEST (Figs. 5, 7, and S8). Still, for both sites, the choice of instrumental datasets more significantly affects correlation results and their temporal stability.

Trends of sub-diurnal temperature variables have differed substantially in the YT since 1901. While Tmin steadily increased throughout the 20th century, Tmax remained stable until the 1970s when it started rising sharply (Fig. 6 and S7). Tmean naturally moves between the two parameters but is continuously closer to Tmax, which overall shows greater variance. This phenomenon of asymmetric warming has been observed in various regions and may be related to changes in cloud cover (Wilson and Luckman, 2002) and soil moisture (Zhong et al., 2023). MXD chronologies of NKL and CNY track the trend in Tmax more closely, especially between the 1940s and 1980s when Tmin anomalies are distinctly higher than Tmax. Annual variability is also more closely related to Tmax as shown by considerably higher correlations throughout the whole investigation period which is in line with various dendroclimatic studies from North America (King et al., 2024; Reid et al., 2025; Seftigen et al., 2022; Wilson et al., 2014; Wilson and Luckman, 2003). High solar radiation is typically positively correlated with diurnal temperature range (Campbell and Vonder Haar, 1997), i.e. high Tmax and low Tmin, which may enhance the positive relationship between tree growth and Tmax compared to Tmean in this region. Periods of convergence and divergence between our Tmax and Tmin data are consistent with decreasing and increasing solar radiation during "global dimming" between the 1950s and 1980s (Fig. 6a, b, e, f; Büntgen et al., 2021b; Liepert, 2002) and following "global brightening" (Wild, 2009), phenomena that may also partially explain trends in our moving correlation statistics. While the intensity of "dimming" and "brightening" was regionally heterogeneous (D'Arrigo et al., 2008), data from neighboring regions (Sharma et al., 2004; Stanhill and Callaghan, 1995) suggest that the YT may have been significantly impacted.

4.4. Effects of the Pacific decadal oscillation and extreme drought years

So far, we have identified several methodological factors that systematically affect estimates of climate signals and DP in our TR data. However, it is likely that the climate response of our two sites is additionally influenced by variations in the Pacific Decadal Oscillation (PDO). A shift in the PDO during the 1970s, from a negative (drier) phase to a positive (wetter) one, may have benefitted tree growth (Chavardès et al., 2013) which might explain the sharp increase in moving correlation with temperature during this time, especially for the drier CNY site (e.g. Fig. 2d). Although we found no significant long-term relationship between precipitation and density parameters (Fig. S9), latewood formation indeed appears to be negatively affected in years of extreme drought. During the 96 years of which reliable precipitation records exist for the CNY grid cell, 1958 and 1998 had the driest spring and early summer periods (March–July), reaching only 51.8 and 61.6 mm, respectively. Drought conditions in these years are further corroborated by strong wildfire activity with the largest fires close to CNY occurring in the same two years. The 1958 fires burned several thousand square kilometers of forest only 20 km east of the CNY site and the Fox Lake Fire of 1998 affected a similar area (Fig. 8, Government of Yukon, n.d.; Hogg and Wein, 2005). Notably, these anomalies coincide with the two largest negative residuals between reconstructed and measured summer temperatures for both density proxies, with greater deviations for LWBI (3.27 and 2.69 °C) than MXD (2.73 and 1.78 °C). Consequently, correlations with temperature are distinctly weakened in the periods surrounding the drought events. 31-year moving correlations between 1943 and 1973 decrease significantly when compared to a time series in which 1958 values are removed (Fig. 8d–f). While not fully explaining the drop in correlation for LWBI between the 1940s and 1970s, only omitting this one year produces a stable or even increasing trend of MXD correlations during the 20th century. Removing 1998 similarly affects correlation values in recent decades, albeit to a smaller degree. Despite these manipulations not being applicable for a final climate reconstruction, they demonstrate that the climate in parts of the southern Yukon is close enough to semi-arid to negatively affect all TR parameters in anomalously dry years. Again, the temperature signal in MXD appears less impaired by drought than in LWBI. At our northern NKL site, which receives substantially more precipitation than CNY (Fig. 1), none of the three driest years corresponds to a negative residual between MXD and temperature (Fig. S15). Similarly, the regional analysis in Reid et al. (2025) does not show such a growth-limiting effect of drought years, implying that it might be limited to the driest parts of the YT (Chavardès et al., 2013). However, it might still be relevant for the underprediction of extreme warm years such as 1998 in both this and Reid et al.'s (2025) analysis. Although no extremely dry summers have occurred in the last 25 years, rising temperature and evapotranspiration may aggravate this issue in the coming decades, representing a potential cause of DP that may become increasingly relevant.

5. Conclusion

We have performed a comparative analysis of MXD and LWBI data from two sites in the YT to systematically identify potential drivers of divergence and assess their respective impacts. Firstly, SF ADS detrended MXD chronologies consistently delivered the best results compared to other TR proxies and detrending options. Secondly, differences between the BEST and CRU datasets and maximum, minimum, and mean temperatures emphasized the importance of thorough target selection, with BEST Tmax proving to be the optimal choice for our sites. For the southern site CNY, an investigation of two drought years highlighted hydroclimate as an additional cause of non-linear proxy-temperature relationships, possibly connected with the PDO. Overall, both sample sites have retained strong relationships with interannual summer temperature variability but their ability to capture the modern warming trend is limited. This result confirms observations made in Briffa et al.'s (1998) groundbreaking study for NWNA while also incorporating the three most recent decades of accelerated temperature increase. Although our findings do not finally resolve DP, our approach may offer a useful framework for assessing non-stationary growth responses in other regions and identifying contributing factors. Reid et al. (2025), utilizing a broader network of sites across their larger Yukon network, showed that higher elevation, near tree-line locations provided a more stable relationship between LWBI and temperature than the LWBI data used in this analysis. Thus, it is likely that, despite the robust and stable temperature signal in our MXD data, selecting more optimal sites could further minimize DP and improve tree-ring based temperature reconstructions in the YT.

Authors statement

M.K., R.W., and J.E. conceived and planned the study. M.K.

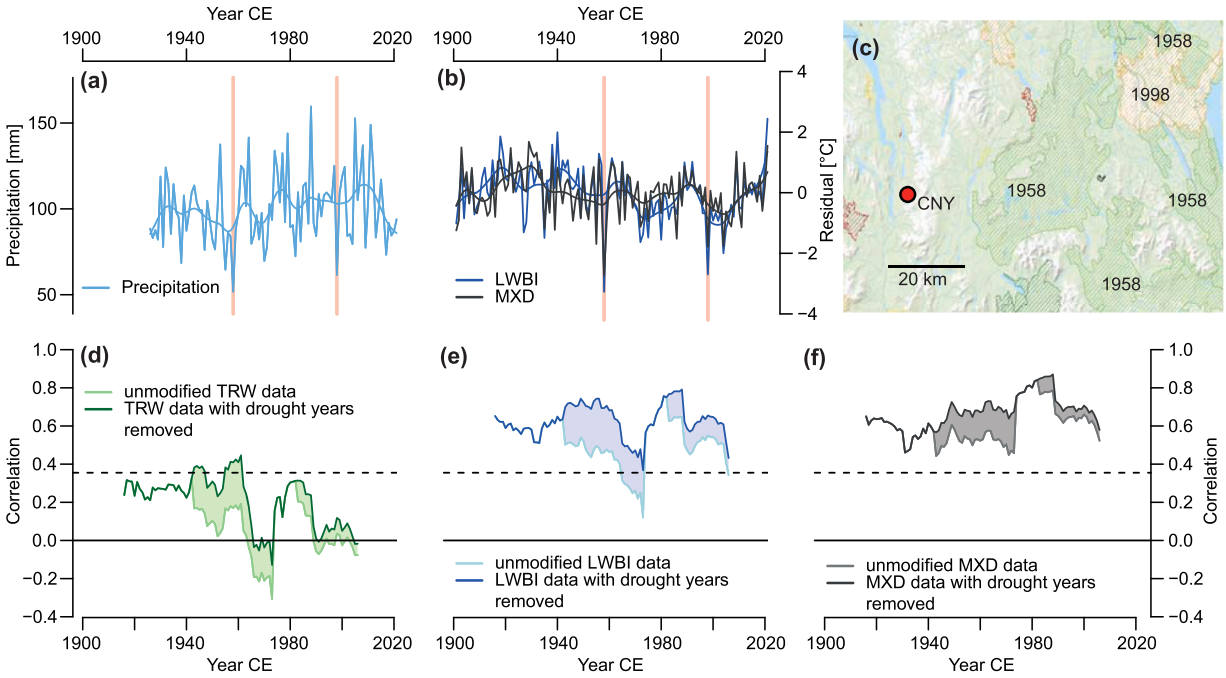

Fig. 8. Influence of drought on temperature signals at CNY considering spring and early summer precipitation (March–July) with red bars indicating 1958 and 1998 (a), residuals between May–August Tmax and proxy chronologies scaled over the whole period (b), map of larger-scale wildfires (c), and effect of drought year removal on 31-year moving correlations using May–August Tmax against TRW (d), LWBI (e), and MXD (f).

conducted the analysis and drafted the manuscript with support from R. W., J.E., E.R., and E.K. All authors provided discussion and agreed to the final version of the manuscript.

CRediT authorship contribution statement

Eileen Kuhl: Writing – review & editing. **Emily Reid:** Writing – review & editing. **Rob Wilson:** Writing – review & editing, Supervision, Methodology, Conceptualization. **Marcel Kunz:** Writing – original draft, Methodology, Formal analysis, Conceptualization. **Jan Esper:** Writing – review & editing, Supervision, Methodology, Funding acquisition, Conceptualization.

Funding

This work was supported by the ERC Advanced Grant (# 882727; Monostar), the Czech Science Foundation grant HYDRO8 (23–08049S), the co-funded EU project AdAgriF (# CZ.02.01.01/00/22_008/0004635), and the ERC Synergy Grant (# 101118880; Synergy-Plague). Emily Reid's PhD was funded through the Carnegie Trust of Scotland.

Declaration of Competing Interest

The authors declare that they have no known competing financial interests or personal relationships that could have appeared to influence the work reported in this paper.

Acknowledgements

We thank the Tr'ondëk Hwëch'in, Na-Cho Nyäk Dun, as well as the Champagne and Aishihik First Nations for their permission to conduct this research on their land. We also thank Lisa Kinder, Julia Haber, and Markus Kochbeck for laboratory support. Finally, we thank three anonymous reviewers whose insightful comments helped improve the manuscript.

Appendix A. Supporting information

Supplementary data associated with this article can be found in the online version at doi:10.1016/j.dendro.2025.126399.

Data availability

The tree-ring data and meta information are available upon request to the authors and will be submitted to the International Tree-Ring Databank (ITRDB) after publication.

References

Allen, K.J., Villalba, R., Lavergne, A., Palmer, J.G., Cook, E.C., Fenwick, P., Drew, D.M., Turney, C.S.M., Baker, P.J., 2018. A comparison of some simple methods used to detect unstable temperature responses in tree-ring chronologies. Dendrochronologia 48, 52–73. https://doi.org/10.1016/j.dendro.2018.02.002.

Babst, F., Frank, D., Büntgen, U., Nievergelt, D., Esper, J., 2009. Effect of sample preparation and scanning resolution on the blue reflectance of picea abies. Tree Rings Archaeol. Climatol. Ecol. 7, 188–195.

Barber, V.A., Juday, G.P., Finney, B.P., 2000. Reduced growth of alaskan White spruce in the twentieth century from temperature-induced drought stress. Nature 405, 668–673. https://doi.org/10.1038/35015049.

Björklund, J., Arx, G., Nievergelt, D., Wilson, R., van den Bulcke, J., Günther, B., Loader, N.J., Rydval, M., Fonti, P., Scharnweber, T., Andreu–Hayles, L., Büntgen, U., D'Arrigo, R., Davi, N., de Mil, T., Esper, J., Gärtner, H., Geary, J., Gunnarson, B.E., Hartl, C., Hevia, A., Song, H., Janecka, K., Kaczka, R.J., Kirdyanov, A.V., Kochbeck, M., Liu, Y., Meko, M., Mundo, I., Nicolussi, K., Oelkers, R., Pichler, T., Sánchez–Salguero, R., Schneider, L., Schweingruber, F., Timonen, M., Trouet, V., van Acker, J., Verstege, A., Villalba, R., Wilmking, M., Frank, D., 2019. Scientific merits and analytical challenges of Tree–Ring densitometry. Rev. Geophys 57, 1224–1264. https://doi.org/10.1029/2019RG000642.

Björklund, J.A., Gunnarson, B.E., Seftigen, K., Esper, J., Linderholm, H.W., 2014. Blue intensity and density from Northern fennoscandian tree rings, exploring the potential to improve summer temperature reconstructions with earlywood information. Clim 10, 877–885. https://doi.org/10.5194/cp-10-877-2014.

Björklund, J., Gunnarson, B.E., Seftigen, K., Zhang, P., Linderholm, H.W., 2015. Using adjusted blue intensity data to attain high-quality summer temperature information: a case study from central scandinavia. Holocene 25, 547–556. https://doi.org/10.1177/0959683614562434.

Björklund, J., Seftigen, K., Kaczka, R.J., Rydval, M., Wilson, R., 2024. A definition and standardised terminology for blue intensity from conifers. Dendrochronologia 85, 126200. https://doi.org/10.1016/j.dendro.2024.126200.

Briffa, K.R., Jones, P.D., Bartholin, T.S., Eckstein, D., Schweingruber, F.H., Karlén, W., Zetterberg, P., Eronen, M., 1992. Fennoscandian summers from ad 500: temperature changes on short and long timescales. Clim. Dyn. 7, 111–119. https://doi.org/10.1007/BF00211153.

Briffa, K.R., Osborn, T.J., Schweingruber, F.H., Harris, I.C., Jones, P.D., Shiyatov, S.G., Vaganov, E.A., 2001. Low-frequency temperature variations from a Northern tree ring density network. J. Geophys. Res. Atmospheres 106, 2929–2941. https://doi.org/10.1029/2000JD900617.

Briffa, K.R., Schweingruber, F.H., Jones, P.D., Osborn, T.J., Shiyatov, S.G., Vaganov, E.A., 1998. Reduced sensitivity of recent tree-growth to temperature at high Northern latitudes. Nature 391, 678–682. https://doi.org/10.1038/35596.

Bunn, A.G., 2008. A dendrochronology program library in r (dplR). Dendrochronologia 26, 115–124. https://doi.org/10.1016/j.dendro.2008.01.002.

Büntgen, U., Allen, K., Anchukaitis, K.J., Arseneault, D., Boucher, É., Bräuning, A., Chatterjee, S., Cherubini, P., Churakova (Sidorova), O.V., Corona, C., Gennaretti, F., Grießinger, J., Guillet, S., Guiot, J., Gunnarson, B., Helama, S., Hochreuther, P., Hughes, M.K., Huybers, P., Kirdyanov, A.V., Krusic, P.J., Ludescher, J., Meier, W.J.-H., Myglan, V.S., Nicolussi, K., Oppenheimer, C., Reinig, F., Salzer, M.W., Seftigen, K., Stine, A.R., Stoffel, M., St. George, S., Tejedor, E., Trevino, A., Trouet, V., Wang, J., Wilson, R., Yang, B., Xu, G., Esper, J., 2021a. The influence of decision-making in tree ring-based climate reconstructions. Nat. Commun. 12, 3411. https://doi.org/10.1038/s41467-021-23627-6.

Büntgen, U., Frank, D., Wilson, R., Carrer, M., Urbinati, C., Esper, J., 2008. Testing for tree-ring divergence in the european Alps. Glob. Change Biol. 14, 2443–2453. https://doi.org/10.1111/j.1365-2486.2008.01640.x.

Büntgen, U., Kirdyanov, A.V., Krusic, P.J., Shishov, V.V., Esper, J., 2021b. Arctic aerosols and the 'Divergence Problem' in dendroclimatology. Dendrochronologia 67, 125837. https://doi.org/10.1016/j.dendro.2021.125837.

Büntgen, U., Wilson, R., Wilmking, M., Niedzwiedz, T., Bräuning, A., 2009. The 'Divergence Problem' in tree-ring research. TRACE–Tree Rings Archaeol. Climatol. Ecol. Vol. 7 7, 212–219. Proc. DENDROSYMPOSIUM 2008 April 27th30th 2008 Zakop. Pol. GFZ Potsdam Sci. Tech. Rep.

Campbell, G.G., Vonder Haar, T.H., 1997. Comparison of surface temperature minimum and maximum and satellite measured cloudiness and radiation budget. J. Geophys. Res. Atmospheres 102, 16639–16645. https://doi.org/10.1029/96JD02718.

Chavardès, R.D., Daniels, L.D., Waeber, P.O., Innes, J.L., Nitschke, C.R., 2013. Unstable climate−growth relations for White spruce in southwest Yukon, Canada. Clim. Change 116, 593–611. https://doi.org/10.1007/s10584-012-0503-8.

Coates, K.S., Morrison, W.R., 2015. The Alaska highway in world war II: the U.S. Army of occupation in Canada's northwest. University of Oklahoma Press.

Cook, E.R., 1985. A Time Series Analysis Approach to Tree Ring Standardization. University of Arizona.

Cook, E.R., Briffa, K.R., Meko, D.M., Graybill, D.A., Funkhouser, G., 1995. The "segment length curse" in long tree-ring chronology development for palaeoclimatic studies. Holocene 5, 229–237. https://doi.org/10.1177/095968369500500211.

Cook, E.R., Krusic, P.J., Peters, K., Holmes, R.L., 2017a. Program ARSTAN (49v1b_MRWE), Autoregressive tree–ring standardization program.

Cook, E.R., Krusic, P.J., Peters, K., Holmes, R.L., 2017b. Program Signal Free (version 45_v2b), RCS Signal Free tree-ring standardization program.

R. Core Team, 2023. R: A Language and Environment for Statistical Computing.

Cuny, H.E., Rathgeber, C.B.K., Frank, D., Fonti, P., Fournier, M., 2014. Kinetics of tracheid development explain conifer tree-ring structure. N. Phytol. 203, 1231–1241. https://doi.org/10.1111/nph.12871.

D'Arrigo, R., Davi, N., Jacoby, G., Wilson, R., Wiles, G., 2014. Dendroclimatic Studies: Tree Growth and Climate Change in Northern Forests, Dendroclimatic Studies: Tree Growth and Climate Change in Northern Forests. https://doi.org/10.1002/9781118848548.ch6.

D'Arrigo, R.D., Kaufmann, R.K., Davi, N., Jacoby, G.C., Laskowski, C., Myneni, R.B., Cherubini, P., 2004. Thresholds for warming-induced growth decline at elevational tree line in the Yukon territory, Canada. Glob. Biogeochem. Cycles 18, GB3021. https://doi.org/10.1029/2004GB002249.

D'Arrigo, R., Wilson, R., Liepert, B., Cherubini, P., 2008. On the 'Divergence Problem' in Northern forests: a review of the tree-ring evidence and possible causes. Glob. Planet. Change 60, 289–305. https://doi.org/10.1016/j.gloplacha.2007.03.004.

Driscoll, W.W., Wiles, G.C., D'Arrigo, R.D., Wilmking, M., 2005. Divergent tree growth response to recent climatic warming, lake clark national park and preserve, Alaska. Geophys. Res. Lett. 32. https://doi.org/10.1029/2005GL024258.

Esper, J., Cook, E.R., Krusic, P.J., Peters, K., Schweingruber, F.H., 2003. Tests of the RCS method for preserving Low-Frequency variability in long Tree-Ring chronologies. TreeRing Res 59.

Esper, J., Frank, D., 2009. Divergence pitfalls in tree-ring research. Clim. Change 94, 261–266. https://doi.org/10.1007/s10584-009-9594-2.

Esper, J., Frank, D.C., Wilson, R.J.S., Briffa, K.R., 2005. Effect of scaling and regression on reconstructed temperature amplitude for the past millennium. Geophys. Res. Lett. 32. https://doi.org/10.1029/2004GL021236.

Esper, J., Klippel, L., Krusic, P.J., Konter, O., Raible, C.C., Xoplaki, E., Luterbacher, J., Büntgen, U., 2020. Eastern Mediterranean summer temperatures since 730 CE from mt. Smolikas tree-ring densities. Clim. Dyn. 54, 1367–1382. https://doi.org/10.1007/s00382-019-05063-x.

Esper, J., Krusic, P.J., Ljungqvist, F.C., Luterbacher, J., Carrer, M., Cook, E., Davi, N.K., Hartl-Meier, C., Kirdyanov, A., Konter, O., Myglan, V., Timonen, M., Treydte, K., Trouet, V., Villalba, R., Yang, B., Büntgen, U., 2016. Ranking of tree-ring based temperature reconstructions of the past millennium. Quat. Sci. Rev. 145, 134–151. https://doi.org/10.1016/j.quascirev.2016.05.009.

Esper, J., Niederer, R., Bebi, P., Frank, D., 2008. Climate signal age effects—evidence from young and old trees in the Swiss engadin. For. Ecol. Manag 255, 3783–3789. https://doi.org/10.1016/j.foreco.2008.03.015.

Esper, J., Schneider, L., Smerdon, J.E., Schöne, B.R., Büntgen, U., 2015. Signals and memory in tree-ring width and density data. Dendrochronologia 62–70. https://doi.org/10.1016/j.dendro.2015.07.001.

Frank, D.C., Büntgen, U., Böhm, R., Maugeri, M., Esper, J., 2007. Warmer early instrumental measurements versus colder reconstructed temperatures: shooting at a moving target. Quat. Sci. Rev. 26, 3298–3310. https://doi.org/10.1016/j.quascirev.2007.08.002.

Fritts, H.C., 1971. Dendroclimatology and dendroecology. Quat. Res. 1, 419–449. https://doi.org/10.1016/0033-5894(71)90057-3.

Fritts, H.C., 1976. Tree Rings and Climate. Elsevier Science, Tucson.

Fuentes, M., Salo, R., Björklund, J., Seftigen, K., Zhang, P., Gunnarson, B., Aravena, J.-C., Linderholm, H.W., 2018. A 970-year-long summer temperature reconstruction from rogen, west-central Sweden, based on blue intensity from tree rings. Holocene 28, 254–266. https://doi.org/10.1177/0959683617721322.

Glock, W.S., 1937. Principles and Methods of Tree-ring Analysis. Carnegie Institution of Washington.

Government of Yukon, n.d. Fire history - Overview [WWW Document]. URL https://yukon.maps.arcgis.com/home/item.html?id=f9588f95c62e4bf69ef02145d91c92ab (Accessed 11.11.24).

Griesbauer, H.P., Green, D.S., 2012. Geographic and temporal patterns in White spruce climate–growth relationships in Yukon, Canada. For. Ecol. Manag 267, 215–227. https://doi.org/10.1016/j.foreco.2011.12.004.

Harris, I., Osborn, T.J., Jones, P., Lister, D., 2020. Version 4 of the CRU TS monthly high-resolution gridded multivariate climate dataset. Sci. Data 7, 109. https://doi.org/10.1038/s41597-020-0453-3.

Heeter, K.J., Harley, G.L., Maxwell, J.T., Wilson, R.J., Abatzoglou, J.T., Rayback, S.A., Rochner, M.L., Kitchens, K.A., 2021. Summer temperature variability since 1730 CE across the low-to-mid latitudes of western North America from a tree ring blue intensity network. https://doi.org/10.1016/j.quascirev.2021.107064.

Higuchi, T., 1997. Formation of earlywood, latewood, and heartwood. In: Higuchi, T. (Ed.), Biochemistry and Molecular Biology of Wood. Springer, Berlin, Heidelberg, pp. 291–307. https://doi.org/10.1007/978-3-642-60469-0_6.

Hogg, E.H. (Ted), Wein, R.W., 2005. Impacts of drought on forest growth and regeneration following fire in southwestern Yukon, Canada. Can. J. For. Res. 35. https://doi.org/10.1139/x05-120.

Holmes, R.L., 1983. Computer-assisted quality control in tree-ring dating and measurement. TreeRing Bull. 43, 69–78.

Homfeld, I.K., Büntgen, U., Reinig, F., Torbenson, M.C.A., Esper, J., 2024. Application of RCS and signal-free RCS to tree-ring width and maximum latewood density data. Dendrochronologia 85, 126205. https://doi.org/10.1016/j.dendro.2024.126205.

Jacoby, G.C., Cook, E.R., 1981. Past temperature variations inferred from a 400-Year Tree-Ring chronology from Yukon territory, Canada. Arct. Alp. Res. 13, 409–418. https://doi.org/10.2307/1551051.

Jacoby, G.C., D'Arrigo, R.D., 1995. Tree ring width and density evidence of climatic and potential forest change in Alaska. Glob. Biogeochem. Cycles 9, 227–234. https://doi.org/10.1029/95GB00321.

Jätzold, R., 2000. Semi-arid regions of the boreal zone as demonstrated in the Yukon basin. Erdkunde 54, 1–19. https://doi.org/10.3112/erdkunde.2000.01.01.

Jevšenak, J., Levanič, T., 2018. dendroTools: r package for studying linear and nonlinear responses between tree-rings and daily environmental data. Dendrochronologia 48, 32–39. https://doi.org/10.1016/j.dendro.2018.01.005.

Kaczka, R.J., Wilson, R., 2021. I-BIND: international blue intensity network development working group. Dendrochronologia 68, 125859. https://doi.org/10.1016/j.dendro.2021.125859.

King, K.E., Harley, G.L., Maxwell, J.T., Rayback, S., Cook, E., Maxwell, R.S., Rochner, M.L., Bergan, E.V., Foley, Z., Therrell, M., Bregy, J., 2024. Reconstructed late summer maximum temperatures for the southeastern United States from Tree-Ring blue intensity. Geophys. Res. Lett. 51, e2024GL109099. https://doi.org/10.1029/2024GL109099.

Kirdyanov, A.V., Krusic, P.J., Shishov, V.V., Vaganov, E.A., Fertikov, A.I., Myglan, V.S., Barinov, V.V., Browse, J., Esper, J., Ilyin, V.A., Knorre, A.A., Korets, M.A., Kukarskikh, V.V., Mashukov, D.A., Onuchin, A.A., Piermattei, A., Pimenov, A.V., Prokushkin, A.S., Ryzhkova, V.A., Shishikin, A.S., Smith, K.T., Taynik, A.V., Wild, M., Zorita, E., Büntgen, U., 2020. Ecological and conceptual consequences of Arctic pollution. Ecol. Lett. 23, 1827–1837. https://doi.org/10.1111/ele.13611.

Konter, O., Büntgen, U., Carrer, M., Timonen, M., Esper, J., 2016. Climate signal age effects in boreal tree-rings: lessons to be learned for paleoclimatic reconstructions. Quat. Sci. Rev. 142, 164–172. https://doi.org/10.1016/j.quascirev.2016.04.020.

Lawrimore, J.H., Menne, M.J., Gleason, B.E., Williams, C.N., Wuertz, D.B., Vose, R.S., Rennie, J., 2011. An overview of the global historical climatology network monthly mean temperature data set, version 3. J. Geophys. Res. Atmospheres 116. https://doi.org/10.1029/2011JD016187.

Leland, C., Davi, N., D'Arrigo, R., Andreu-Hayles, L., Pacheco-Solana, A., Edwards, J., Anchukaitis, K.J., Porter, T.J., Pisaric, M.F.J., Mant, M., Galloway, T., Oelkers, R., 2025. Tree-ring evidence of the elusive 1959 summer cold event in northwestern North America. Arct. Antarct. Alp. Res. 57, 2445945. https://doi.org/10.1080/15230430.2024.2445945.

Liepert, B.G., 2002. Observed reductions of surface solar radiation at sites in the United States and worldwide from 1961 to 1990, 61-1-61–4 Geophys. Res. Lett. 29. https://doi.org/10.1029/2002GL014910.

Lloyd, A.H., Fastie, C.L., 2002. Spatial and temporal variability in the growth and climate response of treeline trees in Alaska. Clim. Change 52, 481–509. https://doi.org/10.1023/A:1014278819094.

Loehle, C., 2009. A mathematical analysis of the divergence problem in dendroclimatology. Clim. Change 94, 233–245. https://doi.org/10.1007/s10584-008-9488-8.
Mankin, K.R., Mehan, S., Green, T.R., Barnard, D.M., 2024. Review of gridded climate products and their use in hydrological analyses reveals overlaps, gaps, and need for more objective approach to model forcings. Hydrol. Earth Syst. Sci. Discuss. 1–36. https://doi.org/10.5194/hess-2024-58.
McCarroll, D., Pettigrew, E., Luckman, A., Guibal, F., Edouard, J.-L., 2002. Blue reflectance provides a surrogate for latewood density of High-latitude pine tree rings. Arct. Antarct. Alp. Res. 34, 450–453. https://doi.org/10.1080/15230430.2002.12003516.
McPartland, M.Y., Dolman, A.M., Laepple, T., 2024. Separating common signal from proxy noise in tree rings. Geophys. Res. Lett. 51, e2024GL109282. https://doi.org/10.1029/2024GL109282.
Melvin, T.M., Briffa, K.R., 2008. A "signal-free" approach to dendroclimatic standardisation. Dendrochronologia 26, 71–86. https://doi.org/10.1016/j.dendro.2007.12.001.
Melvin, T.M., Briffa, K.R., 2014. CRUST: software for the implementation of regional chronology standardisation: part 1. Signal-free RCS. Dendrochronologia 32, 7–20. https://doi.org/10.1016/j.dendro.2013.06.002.
Melvin, T.M., Briffa, K.R., Nicolussi, K., Grabner, M., 2007. Time-varying-response smoothing. Dendrochronologia 25, 65–69. https://doi.org/10.1016/j.dendro.2007.01.004.
Menne, M.J., Williams, C.N., Gleason, B.E., Rennie, J.J., Lawrimore, J.H., 2018. The global historical climatology network monthly temperature dataset, version 4. J. Clim. 31, 9835–9854. https://doi.org/10.1175/JCLI-D-18-0094.1.
Morimoto, D., 2015. Dendroclimatic Studies of White Spruce in the Yukon Territory, Canada. Electron. Thesis Diss. Repos..
Porter, T.J., Pisaric, M.F.J., 2011. Temperature-growth divergence in White spruce forests of old crow flats, Yukon territory, and adjacent regions of northwestern North America. Glob. Change Biol. 17, 3418–3430. https://doi.org/10.1111/j.1365-2486.2011.02507.x.
Reid, E., Esper, J., Kunz, M., Luckman, B.H., Wilson, R., 2025. Expanding the Yukon tree ring blue intensity network to assess divergence effects and enhance climate reconstructions. Holocene.
Reid, K.A., Reid, D.G., Brown, C.D., 2022. Patterns of vegetation change in Yukon: recent findings and future research in dynamic subarctic ecosystems. Environ. Rev. 30, 380–401. https://doi.org/10.1139/er-2021-0110.
Reid, E., Wilson, R., 2020. Delta blue intensity vs. Maximum density: a case study using pinus uncinata in the pyrenees. Dendrochronologia 61, 125706. https://doi.org/10.1016/j.dendro.2020.125706.
Rinn, F., 2003. TSAP-Win™.
Rohde, R.A., Hausfather, Z., 2020. The Berkeley earth Land/Ocean temperature record. Earth Syst. Sci. Data 12, 3469–3479. https://doi.org/10.5194/essd-12-3469-2020.
Römer, P., Hartl, C., Schneider, L., Bräuning, A., Szymczak, S., Huneau, F., Lebre, S., Reinig, F., Büntgen, U., Esper, J., 2021. Reduced temperature sensitivity of maximum latewood density formation in High-Elevation corsican pines under recent warming. Atmosphere 12, 804. https://doi.org/10.3390/atmos12070804.
Rydval, M., Larsson, L.-Å., McGlynn, L., Gunnarson, B.E., Loader, N.J., Young, G.H.F., Wilson, R., 2014. Blue intensity for dendroclimatology: should we have the blues? Experiments from scotland. Dendrochronologia 32, 191–204. https://doi.org/10.1016/j.dendro.2014.04.003.
Rydval, M., Wilson, R., 2012. The impact of industrial SO 2 pollution on north bohemia conifers. Water Air. Soil Pollut. 223, 5727–5744. https://doi.org/10.1007/s11270-012-1310-6.
Schweingruber, F.H., Bräker, O.U., Schär, E., 1979. Dendroclimatic studies on conifers from central Europe and Great Britain. Boreas 8, 427–452. https://doi.org/10.1111/j.1502-3885.1979.tb00438.x.
Schweingruber, F.H., Briffa, K.R., 1996. Tree-Ring density networks for climate reconstruction. In: Jones, P.D., Bradley, R.S., Jouzel, J. (Eds.), Climatic Variations and Forcing Mechanisms of the Last 2000 Years. Springer, Berlin, Heidelberg, pp. 43–66. https://doi.org/10.1007/978-3-642-61113-1_3.
Seftigen, K., Fonti, M.V., Luckman, B., Rydval, M., Stridbeck, P., von Arx, G., Wilson, R., Björklund, J., 2022. Prospects for dendroanatomy in paleoclimatology – a case study on *Picea engelmannii* from the Canadian rockies. Clim 18, 1151–1168. https://doi.org/10.5194/cp-18-1151-2022.
Sharma, S., Lavoué, D., Cachier, H., Barrie, L.A., Gong, S.L., 2004. Long-term trends of the black carbon concentrations in the Canadian Arctic. J. Geophys. Res. Atmospheres 109. https://doi.org/10.1029/2003JD004331.
Shi, F., Yang, B., Linderholm, H.W., Seftigen, K., Yang, F., Yin, Q., Shao, X., Guo, Z., 2020. Ensemble standardization constraints on the influence of the tree growth trends in dendroclimatology. Clim. Dyn. 54, 3387–3404. https://doi.org/10.1007/s00382-020-05179-5.
Speer, J.H., 2010. Fundamentals of Tree-Ring research, reprint edition. Ed. University of Arizona Press, Tucson.
Stanhill, G., Callaghan, T.V., 1995. Solar irradiance, air pollution and temperature changes in the Arctic. Philos. Trans. Phys. Sci. Eng. 352, 247–258.
Stanhill, G., Cohen, S., 2001. Global dimming: a review of the evidence for a widespread and significant reduction in global radiation with discussion of its probable causes and possible agricultural consequences. Agric. For. Meteor. 107, 255–278. https://doi.org/10.1016/S0168-1923(00)00241-0.
Wells, N., Goddard, S., Hayes, M.J., 2004. A Self-Calibrating palmer drought severity index. J. Clim. 17, 2335–2351. https://doi.org/10.1175/1520-0442(2004)017<2335:ASPDSI>2.0.CO;2.
Wigley, T.M.L., Briffa, K.R., Jones, P.D., 1984. On the average value of correlated time series, with applications in dendroclimatology and hydrometeorology. J. Appl. Meteorol. Clim. 23, 201–213. https://doi.org/10.1175/1520-0450(1984)023<0201:OTAVOC>2.0.CO;2.
Wild, M., 2009. Global dimming and brightening: a review. J. Geophys. Res. Atmospheres 114. https://doi.org/10.1029/2008JD011470.
Wilmking, M., Scharnweber, T., van der Maaten-Theunissen, M., van der Maaten, E., 2017. Reconciling the community with a concept—The uniformitarian principle in the dendro-sciences. Dendrochronologia 44, 211–214. https://doi.org/10.1016/j.dendro.2017.06.005.
Wilmking, M., Singh, J., 2008. Eliminating the "divergence problem" at Alaska's northern treeline. https://doi.org/10.5194/cpd-4-741-2008.
Wilson, R., Allen, K., Baker, P., Boswijk, G., Buckley, B., Cook, E., D'Arrigo, R., Druckenbrod, D., Fowler, A., Grandjean, M., Krusic, P., Palmer, J., 2021. Evaluating the dendroclimatological potential of blue intensity on multiple conifer species from Tasmania and New Zealand. Biogeosciences 18, 6393–6421. https://doi.org/10.5194/bg-18-6393-2021.
Wilson, R., Anchukaitis, K., Andreu-Hayles, L., Cook, E., D'Arrigo, R., Davi, N., Haberbauer, L., Krusic, P., Luckman, B., Morimoto, D., Oelkers, R., Wiles, G., Wood, C., 2019. Improved dendroclimatic calibration using blue intensity in the Southern Yukon. Holocene 29, 1817–1830. https://doi.org/10.1177/0959683619862037.
Wilson, R., D'Arrigo, R., Andreu-Hayles, L., Oelkers, R., Wiles, G., Anchukaitis, K., Davi, N., 2017. Experiments based on blue intensity for reconstructing north pacific temperatures along the gulf of Alaska. Clim 13, 1007–1022. https://doi.org/10.5194/cp-13-1007-2017.
Wilson, R.J.S., Luckman, B.H., 2002. Tree-ring reconstruction of maximum and minimum temperatures and the diurnal temperature range in British Columbia, Canada. Dendrochronologia 20, 257–268. https://doi.org/10.1078/1125-7865-00023.
Wilson, R.J.S., Luckman, B.H., 2003. Dendroclimatic reconstruction of maximum summer temperatures from upper treeline sites in interior British Columbia, Canada. Holocene 13, 851–861. https://doi.org/10.1191/0959683603hl663rp.
Wilson, R., Rao, R., Rydval, M., Wood, C., Larsson, L.-Å., Luckman, B.H., 2014. Blue intensity for dendroclimatology: the BC blues: a case study from British Columbia, Canada. Holocene 24, 1428–1438. https://doi.org/10.1177/0959683614544051.
Youngblut, D., Luckman, B., 2008. Maximum June–July temperatures in the southwest Yukon over the last 300 years reconstructed from tree rings. Dendrochronologia 25, 153–166. https://doi.org/10.1016/j.dendro.2006.11.004.
Zang, C., Biondi, F., 2015. Treeclim: an r package for the numerical calibration of proxy-climate relationships. Ecography 38, 431–436. https://doi.org/10.1111/ecog.01335.
Zhang, Y., Guo, M., Wang, X., Gu, F., Liu, S., 2018. Divergent tree growth response to recent climate warming of abies faxoniana at alpine treelines in east edge of Tibetan plateau. Ecol. Res. 33, 303–311. https://doi.org/10.1007/s11284-017-1538-0.
Zhang, P., Linderholm, H.W., Gunnarson, B.E., Björklund, J., Chen, D., 2016. 1200 years of warm-season temperature variability in central scandinavia inferred from tree-ring density. Clim 12, 1297–1312. https://doi.org/10.5194/cp-12-1297-2016.
Zhong, Z., He, B., Chen, H.W., Chen, D., Zhou, T., Dong, W., Xiao, C., Xie, S., Song, X., Guo, L., Ding, R., Zhang, L., Huang, L., Yuan, W., Hao, X., Ji, D., Zhao, X., 2023. Reversed asymmetric warming of sub-diurnal temperature over land during recent decades. Nat. Commun. 14, 7189. https://doi.org/10.1038/s41467-023-43007-6.